Current Research in Food Science 5 (2022) 1559–1569

Contents lists available at ScienceDirect

Current Research in Food Science

journal homepage: www.sciencedirect.com/journal/current-research-in-food-science

# Proteomic analyses revealed the antibacterial mechanism of *Aronia melanocarpa* isolated anthocyanins against *Escherichia coli* O157: H7

Haotian Deng [a], Yanwen Kong [a], Jinyan Zhu [b], Xinyao Jiao [a], Yuqi Tong [a], Meizhi Wan [a], Yang Zhao [a], Sixu Lin [a], Yan Ma [c], Xianjun Meng [a,*]

[a] College of Food Science, Shenyang Agricultural University, Shenyang, Liaoning Province, 110866, China
[b] Food Inspection Monitoring Center of Zhuanghe, Dalian, Liaoning Province, 116400, China
[c] Center of Experiment Teaching, Shenyang Normal University, Shenyang, Liaoning, 110034, China

ARTICLE INFO

Editor name; Dr. Quancai Sun

*Keywords:*
Aronia melanocarpa
Anthocyanins
TMT proteomic
*Escherichia coli* O157
H7
Response

ABSTRACT

*Aronia melanocarpa* anthocyanins (AMAs), as a natural plant extract, can control pathogens and are attracting increasing attention. However, at the proteomic level, the antibacterial mechanism of AMAs against *Escherichia coli* O157: H7 remains unclear. In this study, the tandem mass tag (TMT) quantitative proteomics was used to elucidate the potential antibacterial mechanisms of AMAs against *E. coli* O157: H7 cells. Ultrastructural observation and reactive oxygen species (ROS) levels detection showed that AMAs destroyed the integrity of *E. coli* O157: H7 cell membrane, led to the aggregation of contents and caused the increase of intracellular ROS level. TMT-based proteomic analysis suggested that AMAs can enter cells through mechanosensitive channels and inhibit the activity of heat shock proteins; disturb the metabolism of carbohydrates, amino acids and lipids in cells. The results of this study provide a reference for the further development of plant-derived antimicrobial agents.

## 1. Introduction

Foodborne pathogens are a serious threat to human life and health, and even low concentrations of pathogenic bacteria pose a high risk to public health (M.-M. Gao et al., 2020; John and Ramaswamy, 2020). *Escherichia coli* O157: H7 is a subset of Shiga toxin-producing bacteria, which is a typical food-borne pathogen with the characteristics of strong pathogenicity, strong drug resistance and wide epidemic (Sengun et al., 2020). It can be transmitted through water, animal foods (including poultry and beef), fruits and vegetables, and poses a serious threat to the health of food processors and consumers (Usaga et al., 2021). Eating lettuce contaminated with *Escherichia coli* O157: H7 has been reported to have caused 210 infections which spread across 36 U.S. states, killing five people (Lim and Ha, 2021). Infection of humans and animals with *E. coli* O157:H7 can cause considerable morbidity and mortality, which has become a public health concern (Sr et al., 2019). It is very important to control this pathogen and prevent possible outbreaks. Antibiotics are a good means of treating bacterial infections, but the widespread use of antibiotics has resulted in a high degree of bacterial resistance and immune response to antibiotic treatment, which rapidly reduces the effectiveness of traditional antibiotics (Lacombe et al., 2013). At the same time, the irregular use of antibiotics has a certain impact on the environment. Therefore, there is an urgent need for researchers to develop effective new antimicrobial agents to prevent and control the spread of foodborne pathogens. Many studies have focused on natural plant extracts, including essential oils and phenols, which are considered the most promising candidates for natural antibiotics (Moreira Gonçalves et al., 2020; Alexandrino et al., 2021; Higbee et al., 2022; Elwira et al., 2020).

The fruit of *Aronia melanocarpa* (AM) is a small dark blue berry, which is rich in dietary fiber, proteins, anthocyanins and other nutrients (Kong et al., 2021; Tan et al., 2021; Zhu et al., 2021). Anthocyanins have the functions of lowering blood sugar, lowering blood lipids, protecting the liver and preventing Alzheimer's disease (Kong et al., 2021; Lingshuai et al., 2018; Tasic et al., 2021). In addition, studies have shown that anthocyanins have inhibitory effects on food-borne pathogens such as *Escherichia coli*, *Staphylococcus aureus*, *Listeria monocytogenes*, and *Pseudomonas aeruginosa* (Denev et al., 2019; Righi et al., 2020). Anthocyanins are secondary metabolites of higher plants, which are safe to use in food. Therefore, the application of anthocyanins as antibacterial

* Corresponding author.
*E-mail address:* mengxjsy@126.com (X. Meng).

https://doi.org/10.1016/j.crfs.2022.09.017
Received 29 June 2022; Received in revised form 12 September 2022; Accepted 14 September 2022
Available online 15 September 2022

agents in food industry has attracted more and more attention. For example, Sun et al. have investigated the inhibitory effect of wild blueberry anthocyanins on four food-borne pathogens, showing that anthocyanins can damage bacterial cell membranes, inhibit the intracellular tricarboxylic acid (TCA) cycle and reduce energy transfer (Sun et al., 2018). Lacombe et al. have found that American cranberry anthocyanins caused the disassembly of the outer membrane of *Escherichia coli* O157: H7 cells, resulting in changes in membrane fluidity (Lacombe et al., 2010). Magdalena et al. have reported that *Aronia melanocapa* extract reduces the integrity of *E. coli* cell membranes and inhibits DNA synthesis in cells (Efenberger-Szmechtyk et al., 2021). However, there are few reports on the effect of AMAs on *E. coli* at the protein level. Tandem mass tags (TMT) proteomics can be used to study the changes of protein expression in cells which are under the different environmental stress. It is an effective method to reflect the stress mechanism of microorganism under these stress conditions (Voigt et al., 2014). The differentially expressed proteins (DEPs) can further clarify the molecular mechanism of the antibacterial effect of AMAs on *Escherichia coli* O157: H7. Understanding the response of *Escherichia coli* O157: H7 to AMAs at the protein level will help to clarify the action mode of antimicrobial agents and determine the target of antibacterial effect of AMAs on *E. coli* cells (Sarengaowa et al., 2019).

In this study, the changes of proteome of *Escherichia coli* O157: H7 after AMAs treatment were studied by using TMT quantitative proteomics method. Both the Gene Ontology (GO) annotation and Kyoto Encyclopedia of Genes and Genomes (KEGG) pathway enrichment analysis were used to analyze the key pathways that revealed DEPs. In addition, the target proteins selected by TMT were verified on protein level by multiple reaction monitoring (MRM) technology. This study provides a reference for the application of natural antibacterial agents.

## 2. Materials and methods

### 2.1. Bacterial strain

The *Escherichia coli* O157: H7 strain (CICC 10389) was deposited in the college of food science, Shenyang Agricultural University (Shenyang, China). Before the experiments, the strain needs to be activated. First, the strain was precultured on Tryptic Soy Agar (TSA) medium (Haibo Biotechnology Co., Ltd.) at 37 °C for 24 h. Next, the strain was transferred to Tryptic Soy Broth (TSB) medium at 37 °C to obtain the suspension.

### 2.2. Preparation of AMAs

The AMAs were prepared as previously described (Deng et al., 2021). *Aronia melanocarpa* (AM) were purchased from Liaoning Fu Kangyuan Black 92 Chokeberry Technology Co., Ltd. (Haicheng, Liaoning, China). The AM fruit was mixed with ethanol solution at the ratio of 1:30 (g/mL) and then squeezed and filtered to obtain the concentrate. The liquid crude extract was freeze-dried to obtain the powder anthocyanin crude extract. The anthocyanins were further isolated and purified by semi-preparative high-performance liquid chromatography (Shanghai Hooyo Instrument & Equipment Co., Ltd, Shanghai, China). The purified liquid was desolvated in vacuum and freeze-dried to obtain powdered *Aronia melanocarpa* anthocyanins (AMAs).

### 2.3. Identification of AMAs

The species and composition of AMAs were identified by liquid chromatography-mass spectrometry (HPLC-MS) (Kong et al., 2021). Dissolve 10 mg of AMAs in methanol (2 mL) and filtered using a 0.22 μm filter for high performance liquid chromatography (HPLC) analysis. The HPLC analysis uses a mass spectrometer (Shimadzu LCMS8050, Shimadzu Scientific Instruments, Inc., Kyoto, Japan). A Diamonsil C18 (250 mm × 5.6 mm, 5 μm) column was used. Mobile phases were 0.1% formic acid in water (A) and acetonitrile (B). Gradient elution method: 0–40 min, B: 0–40%; 40–45 min, B: 40–45%; 45–52 min, B: 0%. Injection volume, 20 μL; flow rate, 0.7 mL/min; Column temperature: 30 °C; Detection wavelength: 520 nm. Parameters in $MS^2$ spectrometry: scanning range, 10–1000 m/z; dry gas pressure, 30 psi; flow rate, 12 L/min; dryer temperature, 350 °C; capillary voltage, 3500 V.

### 2.4. Bacterial culture preparation

The minimum inhibitory concentration (MIC) was determined using a two-fold serial dilution method. The bacterial suspensions ($1 \times 10^6$–$1 \times 10^8$ CFU/mL, 10 μL) were added to 2 mL of TSB containing different concentrations of anthocyanins (0.156, 0.313, 0.625, 1.25, 2.5, 5 and 10 mg/mL) at 37 °C for 24 h. At the same time, a control group was set up, and there was no AMAs in the control group. The group in which microbial growth was not observed was the MIC group (Deng et al., 2021). *E. coli* O157: H7 cells cultured to logarithmic phase were added to TSB containing AMAs and cultured at 37 °C for 2 h. The final concentration of AMAs was 0.313 mg/ml, which was half of the MIC of AMAs on *Escherichia coli* O157: H7 (Deng et al., 2021). The group without AMAs was used as the control group. The cultured cells were centrifuged at 5000 *g* for 10min at 4 °C to collect bacterial cells. The cells were washed twice with 0.01 M PBS (pH 7.4). The samples were frozen with liquid nitrogen and stored in a refrigerator at −80 °C. Three samples in each group were prepared in parallel for proteomic experiments.

### 2.5. Scanning electron microscopy (SEM) and transmission electron microscopy (TEM)

*Escherichia coli* O157: H7 cells were treated with AMAs at final concentration of 1/2 MIC at 37 °C for 2 h. The cells were collected by centrifugation at 5000*g* for 10 min at 4 °C. The control cells were prepared as described above, but in the absence of AMAs. The cells washed with PBS (pH 7.4), fixed with 2.5% glutaraldehyde (GTA), and dehydrated with different gradients of ethanol (30%, 50%, 70%, 80%, 90%, and 100%). The freeze-dried cells were coated with gold, and the ultrastructure was observed by SEM (A Regulus 8100 Hitachi, Tokyo, Japan). The cells were washed with PBS and fixed with 5% GTA and then post-fixed with 1% osmic acid. Dehydrated with alcohol and stained with Saito lead. The samples were sectioned and observed by transmission electron microscopy (HT 7700 Transmission Electron Microscope, Hitachi, Japan).

### 2.6. Protein extraction and reductive alkylation

For protein extraction, 500 μL of lysis buffer was added to *E. coli* O157: H7 cells, and ultrasound was performed in an ice bath for 5 min (pulse on 2 s, pulse off 3 s, power 180 W). After sonication, the supernatant was obtained by centrifugation at 20000*g* for 30 min at 4 °C. The protein was then quantified by Bradford analysis (Bradford, 1976). Dithiothreitol (DTT) was added to the supernatant at a final concentration of 10 mM. The samples were bathed in water at 56 °C for 1 h and then taken out. Iodoacetamide (IAM) was added to the sample to a final concentration of 55 mM, and the sample was allowed to stand for 1 h in a dark room. Then, pre-cooled acetone was added to the sample (the volume ratio of sample to acetone was 1:4) and reacted at −20 °C for 4 h. After the reaction, the mixture was centrifuged at 20000 g for 30 min to obtain precipitation.

### 2.7. Protein trypsin digestion

Add 200 μl triethylammonium bicarbonate (TEAB, 100 Mm) solution to the sample, mix and spin, centrifuge at 14000 *g* at 4 °C for 40 min, and discard the waste liquid. Then, add 1 μg/μL (per 100 μg protein substrate addition 3.3 μg enzyme) to each tube of sample, 37 °C water bath for 24 h. Freeze the dry digestive solution, and then add 25 μl TEAB to each

tube of sample to re dissolve the peptide.

### 2.8. TMT labeling

Add 41 μL acetonitrile to the labeling reagent balanced to room temperature, vortex for 1 min and centrifuge. Add the mixed labeling reagent to the peptide segment, and different samples were labeled with isotopes of different sizes. As shown in Fig. 1, the three samples of the control group were labeled with TMT-130 N, TMT-130 C and TMT-131 respectively; Three samples in the treatment group were labeled with TMT-126, TMT-128 N and TMT-128 C respectively. After mixing, centrifuge to the bottom of the tube and stand for 1 h at room temperature. Add 5% hydroxylamine (8 μL), after 15 min' standing at room temperature, vacuumize to remove the solvents.

### 2.9. Liquid chromatography-mass spectrometry (LC–MS/MS) analysis

Dissolve the peptide into 0.1% (V/V) formic acid (solvent A) and separated with reversed phase C18 column (75μm × 15 cm, 5 μm, 300 Å, Agela Technologies) mounted on a Dionex ultimate 3000 nano LC system. The peptide was eluted at a continuous flow rate of 400 nL/min for 65 min. Solvent B: 0.1% formic acid in 100% acetonitrile. The NanoLC liquid phase gradient in mass spectrometry is shown in Table S1. The eluent was directly fed into Q-Exactive MS (Thermo Fisher Scientific, Waltham, MA, USA), set to positive ion mode and data-dependent mode. The parent ion scanning range is 350–2000 m/Z, the full scanning resolution is 70000, and the MS/MS scanning resolution is 35000. In order to evaluate the performance of the mass spectrum on TMT labeled samples, high collision energy dissociation (HCD) was used.

### 2.10. Database searching and data analysis

The raw data produced from LC-MS/MS were input into proteome discoverer 1.4. Using Mascot (Version: 2.3.01) to search the database, the database is Uniprot-*E.coli* (download time: 2020.04.14, database sequence number: 23139). Carbamidomethyl (C) was used for fixed modifications and oxidation (M) was used for variable modifications.

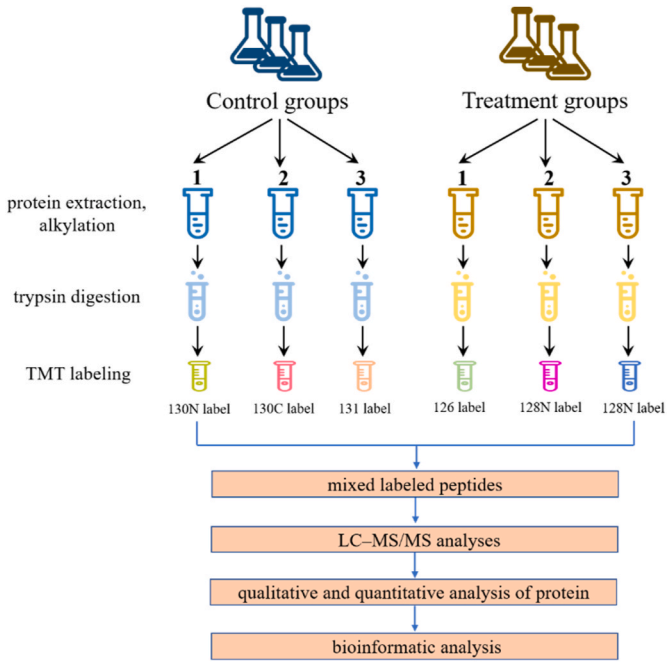


**Fig. 1.** The flow chart of the independent identification of protein profiles from the treatment groups (*Aronia melanocarpa* anthocyanins-treated *Escherichia coli* O157:H7) and the control groups using the tandem mass tagged (TMT).

Trypsin was specified as the cleaving enzyme. The protein database was sourced from http://www.uniprot.org/. FDR <1% was used to filter the results (FDR was the false discovery rate), and the results of peptide and protein identification were obtained. The protein with the number of unique peptide ≥1 was used for subsequent quantitative analysis (X. Gao et al., 2020). Only proteins with the ratios ≥1.5 with P value ≤ 0.05 were set for up-regulation, and the ratios ≤0.67 with P value ≤ 0.05 were set for down-regulation. The Gene Ontology (GO) database (http://www.geneontology.org) divides the identified differentially expressed proteins (DEPs) into three categories: molecular function, cellular component and biological process. The Kyoto Encyclopedia of Genes and Genomes (KEGG) database (http://www.genome.jp/kegg/) analyzed enriched pathways (Li et al., 2018).

### 2.11. Intracellular reactive oxygen species (ROS)

The level of ROS in *Escherichia coli* O157: H7 cells were determined by ROS Assay Kit (Elabscience Biotechnology Co., Ltd.). The dye is 2′,7′-dichlorofluorescein diacetate (DCFH-DA), which is a fluorescent probe that can pass freely through the cell membrane. DCFH-DA can be deacetylated into dichlorofluorescein (DCFH) in the cells. DCFH can be oxidized to 2′, 7′ - dichlorofluorescein (DCF) to reflect the level of ROS in the cells. Briefly, *Escherichia coli* O157: H7 cells ($1 \times 10^8$ CFU/mL) were treated with different concentrations of AMAs at 37 °C for 2h. The cells were washed three times by centrifugation at 5000*g* for 10 min at 4 °C with PBS (pH 7.4), and then resuspended. The *Escherichia coli* O157: H7 cells were incubated with DCFH-DA (the final concentration of 10 mM) at 37 °C for 30 min, washed with PBS for three times and resuspended. Fluorescence intensity was measured by microplate reader (excitation wavelength: 485 nm; emission wavelength: 525 nm). The relative ROS level was expressed as the ratio of fluorescence intensity between the treatment group and the control group (Liu et al., 2018).

### 2.12. Multiple reaction monitoring (MRM) analysis

According to the results of protein identification, MRM method was established by synthesizing the preset targets from TMT. The established MRM method is used to collect the MRM data of the target protein in the samples of the project, and then import the data into Skyline software to extract the MRM peak of the target peptide. It is corrected by the external standard between samples. For the corrected peptide value, take the average value of multiple tests as the quantitative value of peptide. The quantitative values of multiple peptide segments of the same protein are added as the quantitative value of the protein. The *p*-value and ratio of DEPs were calculated by protein quantitative value.

### 2.13. Statistical analysis

All experiments were conducted in triplicate, and the results are expressed as the mean ± standard deviation (SD). One-way analysis of variance (ANOVA) was used for statistical analysis ($P < 0.05$). Statistical software (SPSS version 22.0; IBM, Chicago, IL, USA) was used for data analysis.

## 3. Results and discussion

### 3.1. Anthocyanin composition of AM

HPLC analysis showed that AMAs contained four anthocyanin (cyanidin-3-O-galactoside, cyanidin-3-O-glucoside, cyanidin-3-O-arabinoside, and cyanidin-3-O-xyloside) compounds (Fig. 2). The content of these four anthocyanins in AM accounted for 99.15% (Table 1).

### 3.2. Ultrastructural changes of Escherichia coli O157: H7 cells

The ultrastructural changes of *Escherichia coli* O157: H7 were

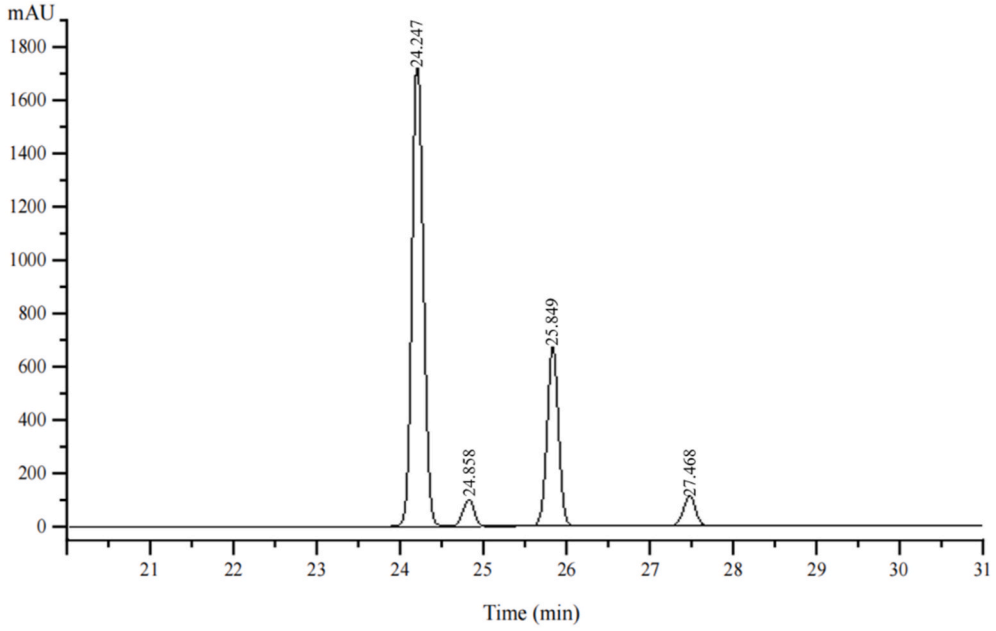


**Fig. 2.** HPLC chromatogram anthocyanins in *Aronia melanocarpa*.

**Table 1**
Identification of anthocyanins in *Aronia melanocarpa* by HPLC-MS.

| Peak number | Anthocyanin name | Retention time (min) | Peak area | Proportion (%) | Molecular (m/z) | fragment (m/z) |
|---|---|---|---|---|---|---|
| 1 | cyanidin-3-O-galactoside | 24.247 | 15999.7 | 65.368 | 449 | 287 |
| 2 | cyanidin-3-O-glucoside | 24.858 | 965.3 | 3.944 | 449 | 287 |
| 3 | cyanidin-3-O-arabinoside | 25.849 | 6148.3 | 25.119 | 419 | 287 |
| 4 | cyanidin-3-O-xyloside | 27.468 | 1154.2 | 4.716 | 419 | 287 |

observed by SEM and TEM. As shown in Fig. 3A, the *E. coli* O157: H7 cells untreated with AMAs showed smooth surface and intact membrane structure. By contrast, the surface of *E. coli* O157: H7 cells treated with AMAs had deformed, some pores (orange arrows), and irregular shrinkage (Fig. 3C). Moreover, TEM showed that the cytoplasm of control group was dense and homogeneous (Fig. 3B). The cells exposed to AMAs (1/2 MIC) were deformed and cytoplasm aggregated (Fig. 3D, green arrows). The results of SEM and TEM showed that AMAs may first destroy the cell membrane and then enter the cell, which may have a certain impact on the homeostasis of the intracellular environment (Ning et al., 2021).

### 3.3. Protein identification and distribution of DEPs

Control and AMAs-treated samples were used for TMT quantitative proteomic analysis. The results showed that 9396 peptides were detected, and 1739 proteins were identified by comparing with the *E. coli* O157: H7 protein database in Uniprot. Differentially expressed proteins indicated proteins with 1.5-fold change and $P < 0.05$. Based on this, 628 DEPs were identified, including 366 up-regulated and 262 down-regulated proteins (Fig. 4A). The heat map of DEPs is shown in Fig. 4B, and each row indicates a protein. The details of each DEP are shown in Table S2. The subcellular localization of each DEP was performed to determine the location of DEPs in cells. As shown in Fig. 4C, of the 628 DEPs, 43.53% were locatedin the Cytoplasm, 7.06% in the cell outer membrane, 2.94% in the cell membrane, 32.94% in the cell inner membrane and 10.29% in the periplasm.

### 3.4. GO analysis of the DEPs

In order to analyze the biological functions of differential proteins between the control and AMAs-treated groups, GO functional annotations were performed on DEPs. Fig. 5 shows three GO functional annotation ranked according to their *p*-value including information on cellular components, molecular functions, and biological processes. Cellular component, membrane, membrane part and integral component of membrane were the four main distributed terms in the cellular component ontology. Other enriched origin categories were intrinsic component of membrane, cell part and cytoplasm (Supporting information: Table S3). Three prevalent molecular functions of DEPs were catalytic activity, binding, heterocyclic compound binding, and organic cyclic compound binding. Ion binding and oxidoreductase activity were also significantly represented (Supporting information: Table S4). The biological processes ontology with the most proteins were cellular processes, metabolic process, organic substance metabolic process, and cellular metabolic process. Others were involved in primary metabolic process, nitrogen compound metabolic process, and biosynthetic process (Supporting information: Table S5).

### 3.5. KEGG pathway enrichment analysis of the DEPs

The pathway enrichment analysis of DEPs was carried out according to KEGG database, and then the metabolic pathway of DEPs was integrated. The differential proteins between the control and AMAs-treated groups were related to 94 KEGG pathways; the first 20 pathways with the lowest *p*-value are shown in Fig. 6. The greater the rich factor, the greater the enrichment. A total of 55 DEPs was involved with biosynthesis of secondary metabolites, 41 with microbial metabolism in diverse environments, 40 with biosynthesis of antibiotics, 29 with two-component system, 26 with biosynthesis of amino acids, and 25 with ABC transporters (Supporting information: Table S6). There are five main categories of KEGG pathways: Genetic Information Processing,

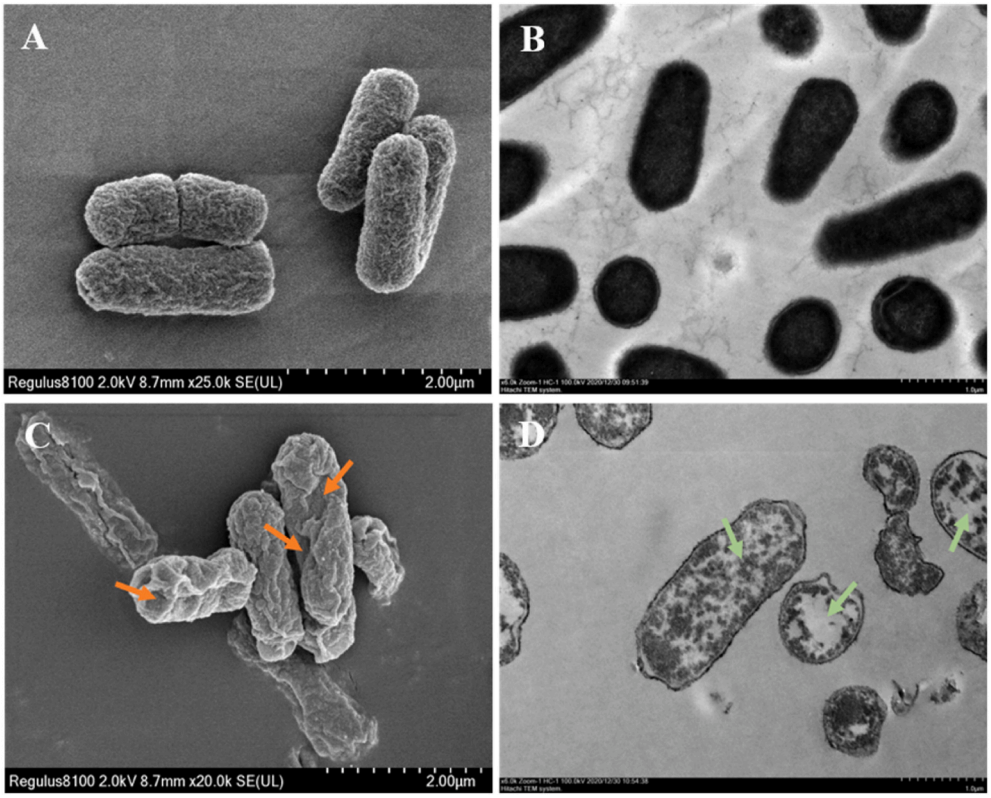


**Fig. 3.** (A) and (C) are SEM images of the control cells, and cells treated with AMAs at 1/2 × MIC, respectively. (B) and (D) are TEM images of the control cells, cells treated with AMAs at 1/2 × MIC, respectively. Orange Arrows: cell surface depression and irregular contraction. Green Arrows: cytoplasmic condensation and intracellular cavity. (For interpretation of the references to color in this figure legend, the reader is referred to the Web version of this article.)

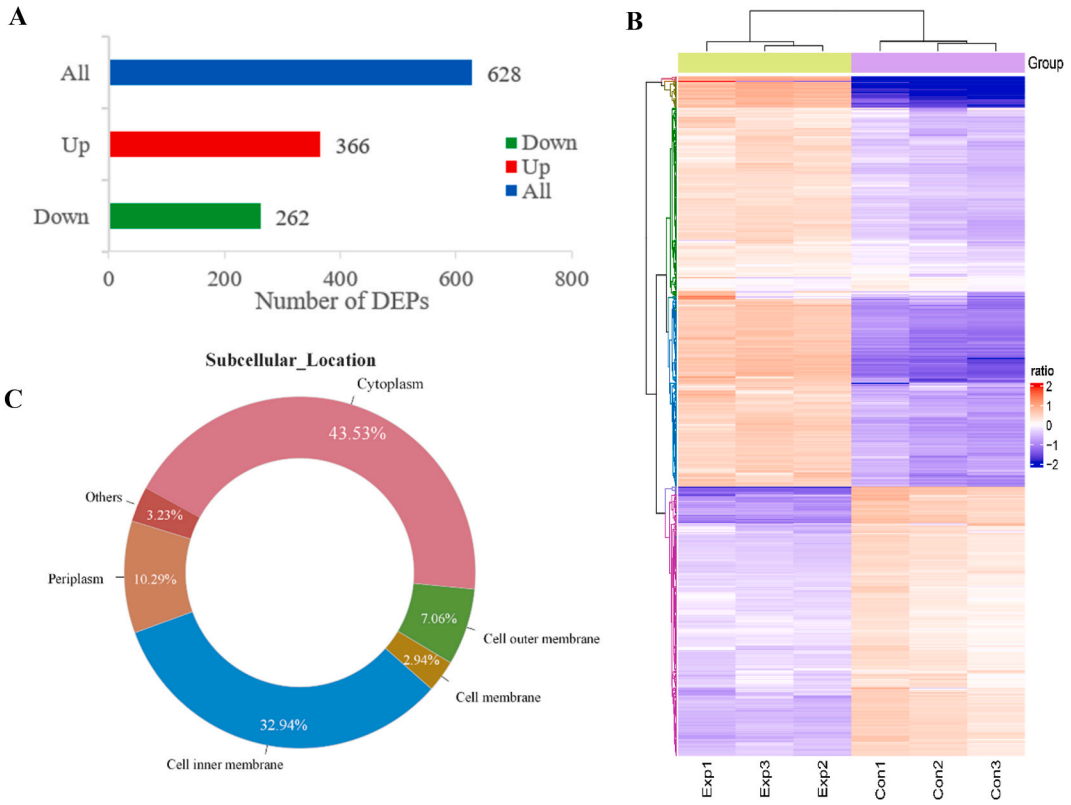


**Fig. 4.** (A) Histogram of DEPs expression level between control cells and AMAs-treated *Escherichia coli* O157:H7; (B) Heat maps of hierarchical clustering analysis of the DEPs between the two groups; (C) Subcellular localization prediction of the DEPs.

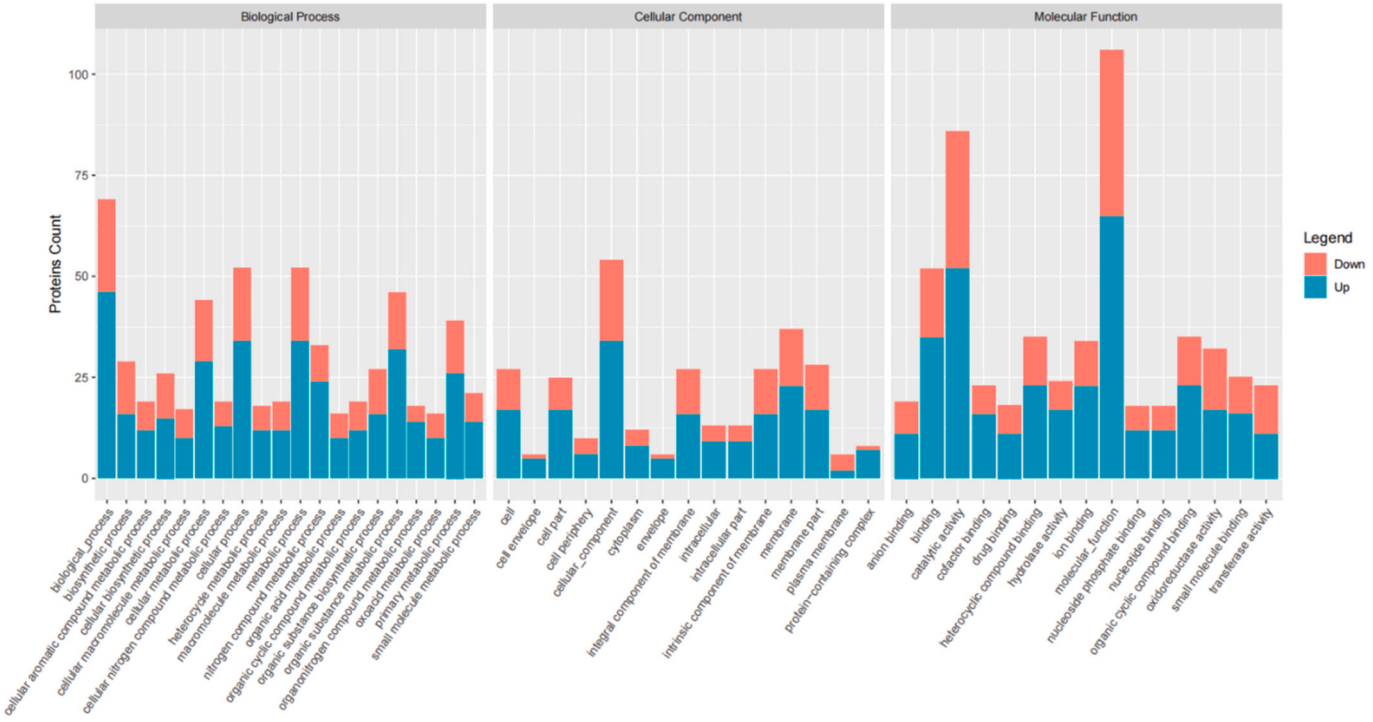


**Fig. 5.** Gene Ontology categories for the differentially expressed proteins. Orange represents down-regulated proteins and indigo represents up-regulated proteins. (For interpretation of the references to color in this figure legend, the reader is referred to the Web version of this article.)

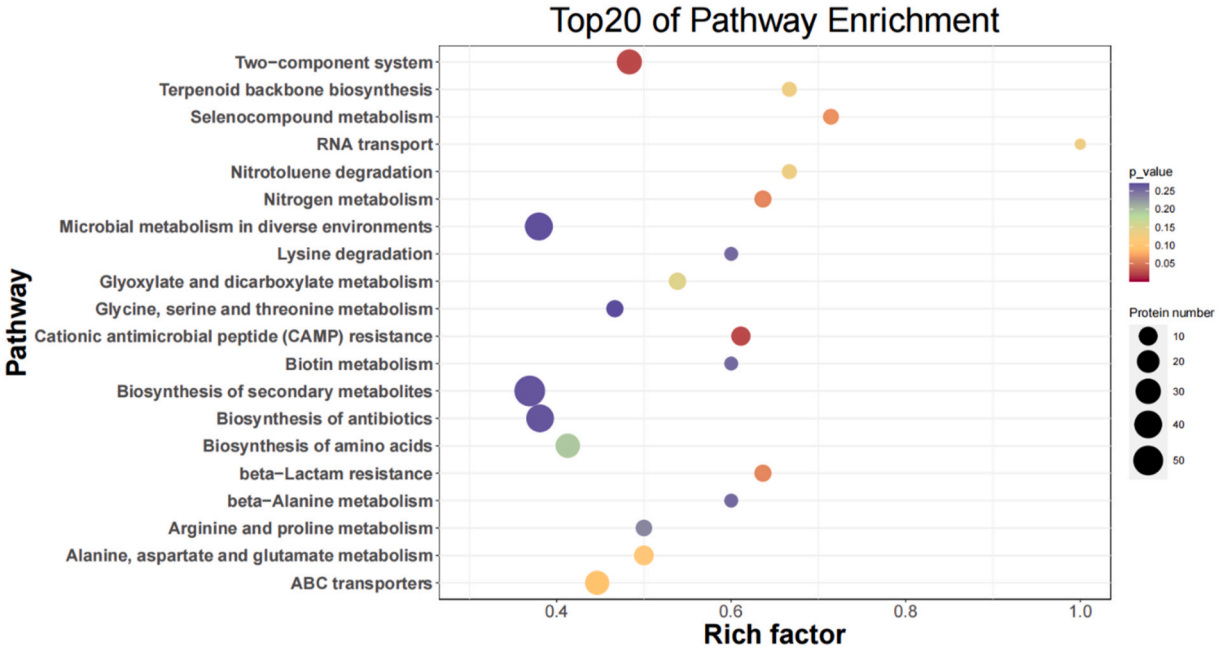


**Fig. 6.** Pathway enrichment analysis of differentially expressed proteins. The abscissa is the rich factor. The greater the rich factor value, the greater the enrichment degree. The ordinate is the name of the metabolic pathway. The color represents the magnitude of the *P* value. The size of the circle represents the amount of protein. (For interpretation of the references to color in this figure legend, the reader is referred to the Web version of this article.)

Cellular Processes, Human Diseases, Environmental Information Processing and Metabolism (Fig. 7). In the metabolism category, the DEPs were mainly distributed in the biosynthesis of secondary metabolites, microbial metabolism in diverse environments, biosynthesis of antibiotics and biosynthesis of amino acids. In the environmental information processing category, the DEPs were mainly distributed in the two-component system, ABC transporters and phosphotransferase system (PTS). In conclusion, AMAs caused various changes of *E. coli* O157: H7 cells, such as mechanical stress, heat shock response, carbohydrate metabolism, energy production, amino acid biosynthesis and metabolism, proteins in lipid metabolism and transport, etc.

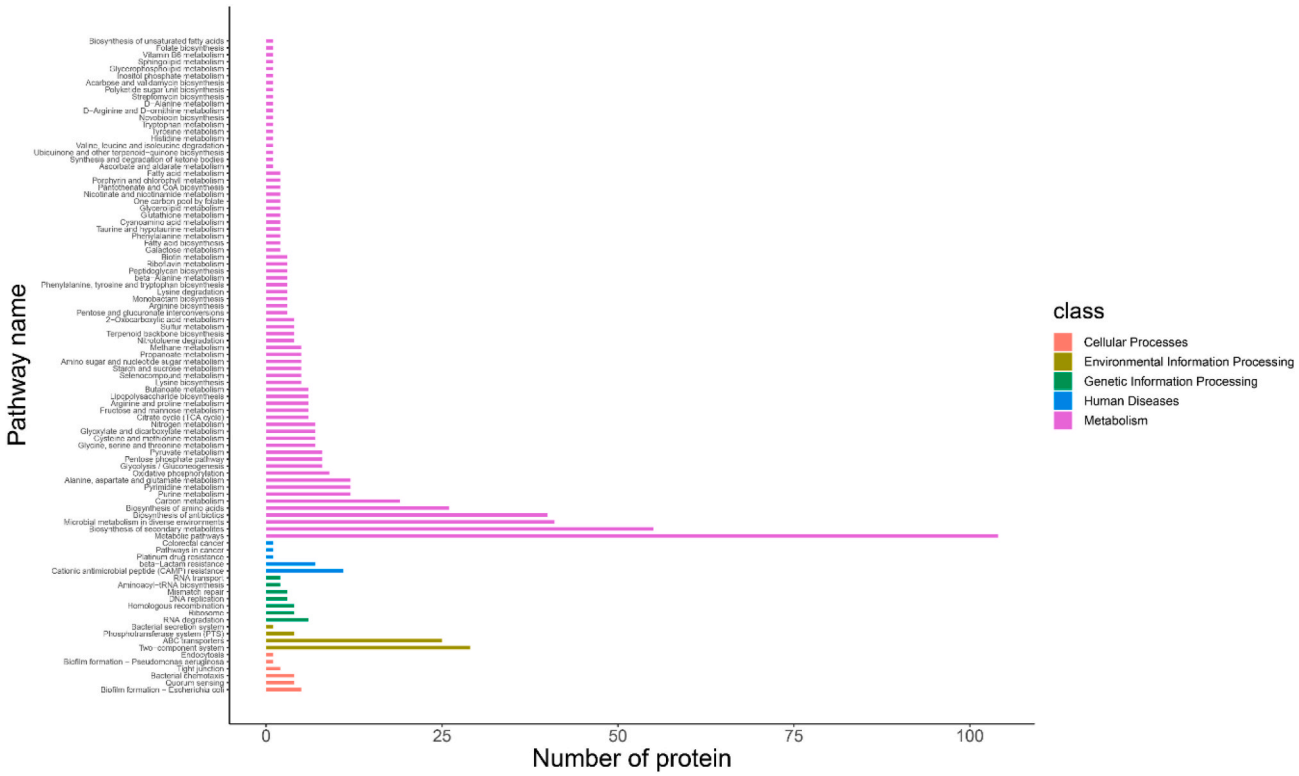


**Fig. 7.** The main categories of KEGG pathways of differentially expressed proteins. The ordinate is the name of the metabolic pathway, and the abscissa is the number of proteins in the metabolic pathway.

### 3.6. Mechanical stress and heat shock response

Bacterial mechanosensitive channel is an ion channel, which can further transmit signals from extracellular to intracellular. These channels are controlled directly by the tensile force of the lipid bilayer (Li et al., 2020). After AMAs treatment, the extracellular environment was changed and large-conductivity mechanosensitive channel (MscL) was activated to relieve intracellular stress. Interestingly, we found that small-conductance mechanosensitive channel (MscS) and low conduct mechanosensitive channel (YnaI) showed down-regulation. The results indicated that *Escherichia coli* O157: H7 cells closed unnecessary channels in order to release intracellular pressure more quickly and prevent AMAs from entering the cells as much as possible. Based on this, we conjecture that AMAs may enter cells through these channels, resulting in the increase of ROS levels, thus causing some disturbance to the metabolism of the intracellular environment. Furthermore, according to the results of intracellular ROS levels determination, we found that ROS level was positively correlated with the concentration of AMAs. (Fig. S1). Thus, cells respond to this disturbance in a variety of ways, including the metabolism and transport of carbohydrates, amino acids, and lipids.

Heat shock protein is a family of proteins produced by cells under stress conditions such as low temperature, ultraviolet light and ultrasound. Heat shock protein binds to many protein molecules. To prevent the proteins that have an effect on the health of cells from interacting with each other (Paes et al., 2019). These proteins also help amino acid chains folding into the correct three-dimensional structure, correct or remove damaged proteins that do not fold properly (Wesche et al., 2009). After AMAs treatment, IbpB is activated to bind to the assembled proteins, protecting them from irreversible aggregation and hydrolysis (Kuczynska-Wisnik et al., 2004). As a companion to heat shock protein, GroES binds to the top of the GroEL ring to form a nanocage that blocks the aggregation of proteins in response to stress, while also promoting and accelerating protein folding (Mogk et al., 2002). GroES and GroEL showed down-regulation, after *Escherichia coli* O157: H7 cells were treated with AMAs, indicating that the binding process of GroES and GroEL was hindered or destroyed. In this study, we also found that the expression of heat shock proteins and chaperones such as HslR, HslO, HtpX, HtpG decreased after AMAs treatment. Normally, when bacterial cells are exposed to stress, heat shock protein and chaperones are activated to protect the cells from the stimulation, which interferes with the metabolism of the internal environment (Li et al., 2020). However, in this study, down-regulation of the most of heat shock proteins indicated that AMAs may directly inhibit the activity of heat shock protein and chaperones, and did not give the bacteria the opportunity to induce a heat shock response to combat this stress.

### 3.7. Carbohydrate metabolic and energy metabolism

The expression of specific proteins in cells increases, under various stress signal states, complete a series of catalytic reactions to resist external stress. This catalytic reaction includes phosphorylation and dephosphorylation. Maltodextrin phosphorylase (MalP) catalyzes the metabolism of maltodextrin to glucose-1-phosphate (G-1-P) and maltodextrin with one less glucose molecule (Watson et al., 1997), were up-regulated after AMAs exposure. In addition, Glycogen phosphorylase (GlgP), which is involved in catalyzing glycogen metabolism, was also shown to be up-regulated after AMAs exposure. These results indicated that cells supplement glucose by increasing substrate phosphorylation levels to promote glycolysis and TCA cycle production of ATP (Fig. 8). Fructose-1-phosphate phosphatase (YqaB) can catalyze the dephosphorylation of fructose 1-phosphate (Fru-1-p); 6-phosphogluconate phosphatase (YieH) catalyzes the dephosphorylation of 6-phosphogluconate (G-6-P), dihydroacetone phosphate (DHAP) and phosphoenolpyruvate (PEP) with the generation of ATP (Kuznetsova et al., 2006). The up-regulation of YqaB and YieH after exposure to AMAs showed that the cells could increase the amount of ATP for growth and reproduction by enhancing the dephosphorylation level of substrate. Aconitate

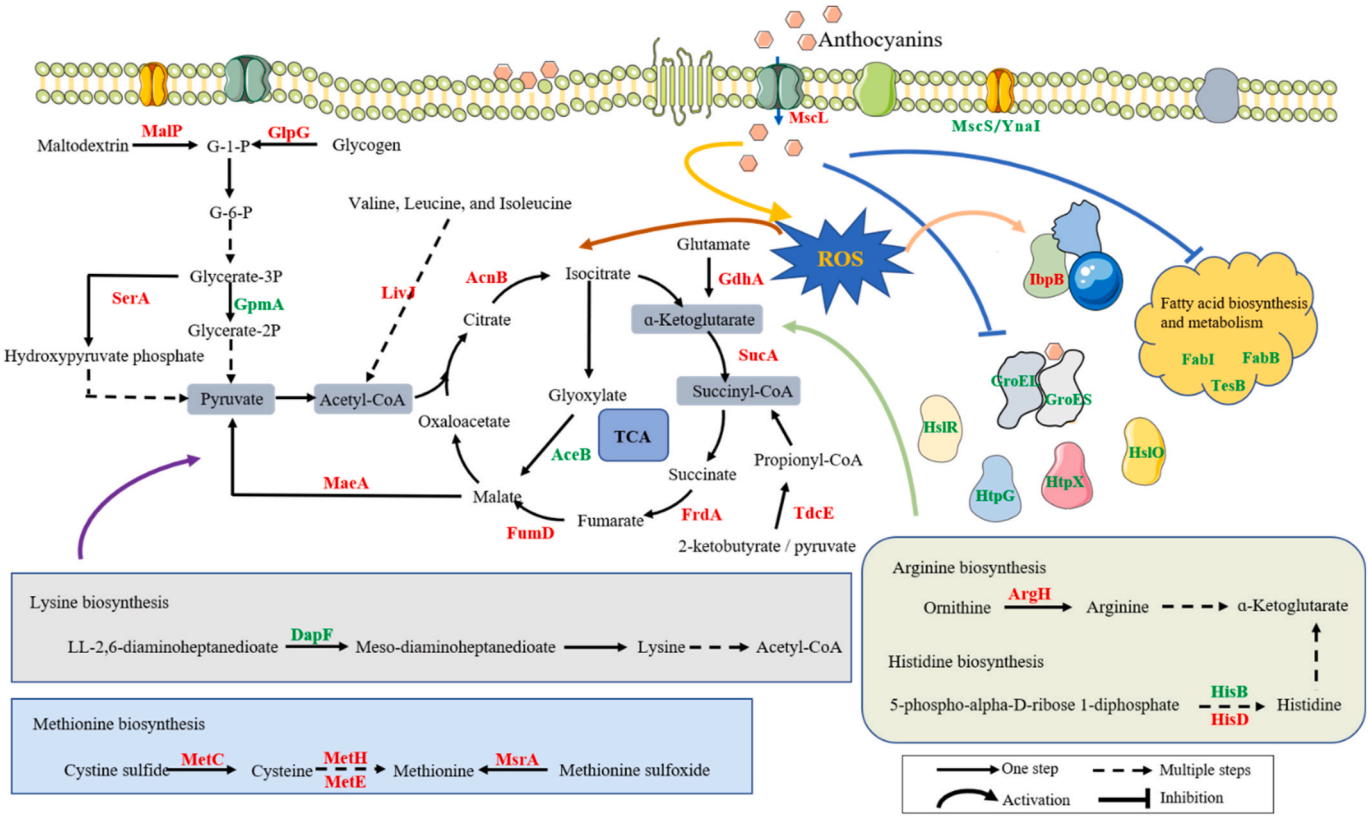


**Fig. 8.** Schematic diagram of regulatory pathways of *Escherichia coli* O157:H7 in response to anthocyanins from *Aronia melanocarpa*.

hydratase B (AcnB) catalyzes the conversion of citric acid to isocitrate to accelerate the occurrence of TCA cycle. Moreover, Malate synthase A (AceB) is responsible for catalyzing the continuous operation of the glyoxylate cycle and improving the ability of organisms to fully utilize acetyl coenzyme A. This cycle can also continuously produce succinic acid to supplement the intermediate metabolites for the TCA cycle (Molina et al., 2010). AcnB was up-regulated and AceB was down-regulated after AMAs exposure, indicating that *E. coli* O157: H7 cells accelerate the production of isocitrate but control the glyoxylate cycle and reduce the utilization level of acetyl-CoA to maintain the TCA cycle. Meanwhile, we found that proteins related to the TCA cycle including 2-oxoglutarate dehydrogenase E1 component (SucA), fumarate reductase flavoprotein subunit (FrdA), and fumarase D (FumD) showed up-regulation. Surprisingly, we found that TdcE, which catalyzes the production of propionyl-CoA, was also up-regulated. Propionyl-CoA can be converted to succinyl-CoA into the TCA cycle (Hesslinger et al., 1998). This result further confirmed that *Escherichia coli* O157: H7 cells fully maintained the TCA cycle under AMAs stress. In addition, the NAD-dependent malic enzyme (MaeA), which catalyzes the conversion of malate to pyruvate, was also shown to be up-regulated. These phenomena further illustrate that *E. coli* O157: H7 cells promote the development of glycolytic process and thus ensure the smooth passage of the TCA cycle. They also speeded up the metabolism of substances such as amino acids to supplement the intermediate metabolites needed for the TCA cycle (Fig. 8).

### 3.8. Amino acid biosynthesis and metabolism

The metabolism of amino acids can protect and repair the bacterial cells that the energy supply of metabolic disorder is insufficient when they under the stress condition (Bi et al., 2017). Argininosuccinate lyase (ArgH) is a key enzyme in the process of catalyzing the synthesis of arginine from ornithine. Arginine is catabolized into α-ketoglutarate and enters the TCA cycle (Kang et al., 2021; Gong et al., 2003). ArgH expression was up-regulated after AMAs treatment. This result suggested that arginine synthesis was increased, and thus the conversion of arginine was accelerated to provide more energy to the cells. The intermediate metabolites of the tricarboxylic acid cycle are supplemented by the reversible oxidative deamination of glutamate. GdhA catalyzes the transamination of glutamate to α-ketoglutarate. After treatment with AMAs, the up-regulation of GdhA expression indicated that *Escherichia coli* O157: H7 cells accelerated glutamate metabolism to ensure the smooth progress of the TCA cycle. Methionine is necessary for bacterial protein biosynthesis. Methionine synthase (MetH) is involved in the sub-pathway of methionine synthesis from cysteine; peptide methionine sulfoxide reductase (MsrA), as a repair enzyme, can catalyze the reversible redox of methionine sulfoxide to methionine in proteins (Vougier et al., 2003). Diaminopimelate epimerase (DapF) catalyzes the lysine biosynthesis pathway and is also an important component of bacterial peptidoglycan. MetH and MsrA, which catalyze methionine biosynthesis, were up-regulated after AMAs treatment, indicating that methionine synthesis was induced by AMAs stress to protect cellular protein synthesis. However, DapF showed down-regulation indicating that lysine biosynthesis was blocked. At the same time, we noticed that the protein HisB involved in histidine biosynthesis was down-regulated and HisD was up-regulated, indicating that the histidine biosynthesis pathway was also disturbed. Leu/Ile/Val-binding protein (LivJ) is a component of the transport system of leucine, isoleucine, and valine. The metabolism of leucine, isoleucine and valine will directly or indirectly increase the synthesis of acetyl-CoA, which has a certain promotion effect on the TCA cycle (Wang et al., 2020). LivJ showed up-regulation in the AMAs-treated group. These results suggest that amino acids may act as protective agents and repair materials to maintain the survival of *Escherichia coli* O157: H7 cells under stress.

### 3.9. Lipid metabolism and transport

Lipids are synthesized and decomposed under the action of various related enzymes, and processed into substances required by the cell body to ensure the normal operation of the cell's physiological function. Lipids are important substances for energy storage and supply of cell bodies, and they are also important components of biofilm structure (Kang et al., 2021). FabI participates in the elongation cycle of fatty acids; FabB catalyzes fatty acid biosynthesis, which is part of fatty acid metabolism. TesB is a thioesterase involved in fatty acid catabolism. It mainly hydrolyzes medium-chain and long-chain acyl-CoA substrates into free fatty acids and CoA, which ultimately serve as energy and carbon precursors for *E. coli* O157: H7 growth (Ohtomo et al., 2013). The expressions of FabI, FabB and TesB were all down-regulated after AMAs treatment, indicating that the fatty acid metabolism in *Escherichia coli* O157: H7 cells was inhibited and the energy supply was affected.

Phospholipids (PLs) are the main components of biological membranes. PLs contain phosphorus to ensure the fluidity and biological functions of membranes. The partial hydrophobicity of phenols enables them to bind to the extracellular membrane, resulting in the change of membrane fluidity (Kwon et al., 2007; Lacombe et al., 2010). The outer membrane of Gram-negative bacteria has asymmetric lipid distribution. Outer leaflet is lipopolysaccharide (LPs) and inner leaflet is PLs. This asymmetric arrangement of lipids has a great significance for the barrier function of bacterial extracellular membrane. When bacterial cells are stimulated by the external environment, PLs will accumulate in outer leaflet, which will have a certain impact on the tissue distribution of LPS, and thus affect the function of extracellular membrane (Malinverni and Silhavy, 2009). Intermembrane phospholipid transport system lipoprotein (MlaA) has a predicted import function to transport PLs from the outer membrane to the inner membrane, maintaining lipid asymmetry in the outer membrane, preventing the accumulation of PLs in the outer leaflet, and being upregulated after AMAs exposure. Lipid A export ATP-binding/permease protein (MsbA) is involved in lipoprotein transport, transferring lipid A from the inner leaflet to the outer leaflet of the inner membrane. MsbA activity was up-regulated after treatment with AMAs, indicating that bacterial cells accelerated lipoprotein transport in order to avoid the interference of AMAs on lipid synthesis.

### 3.10. MRM analysis of the DEPs

Based on TMT quantitative proteomic analysis, we counted and classified some biological process-related DEPs (Table 2). Five proteins with significant changes under AMAs treatment were randomly selected for MRM analysis to verify the proteomic data. These five DEPs include one protein related to heat shock response (B1XDP7), one protein related to energy metabolism (P00363), two proteins related to amino acid biosynthesis and metabolism (P00370, P13009), and one protein related to lipid metabolism and transport (P76506). In the MRM experiments, the protein was quantified using peptide segments to draw a box-plot. Fig. 9 shows the box-plot of five DEPs, one of which show down-regulation (Fig. 9 A) and four proteins showed up-regulation (Fig. 9 B, C, D and E). Overall, the results of MRM and TMT are consistent (Table 3), which more strongly supports the reliability of TMT quantitative proteomics results.

## 4. Conclusion

In conclusion, this study has shown that AMAs has antibacterial activity against *Escherichia coli* O157: H7. Electron microscope images showed that AMAs caused morphological changes and cytoplasmic aggregation of *E. coli* O157: H7 cells. To further understand the response of *E. coli* O157: H7 cells to AMAs stress, we performed TMT quantitative proteomic assays and examined the accumulation of intracellular ROS. The results showed that AMAs induced ROS accumulation after entering the cells and caused oxidative damage to the cells. In order to repair the damage caused by AMAs and ROS, cells actively regulate the expression of related proteins. Furthermore, the MRM verification of randomly selected differential proteins is consistent with the results of TMT proteomics, which proves that the results of TMT quantitative proteomics are reliable. This study provide new insights into the inhibitory mechanisms of natural plant extracts against food-borne pathogens. It also provides a theoretical basis for preventing the tolerance of *Escherichia coli* O157: H7 to antimicrobial drugs.

## Funding

This work was supported by the Liaoning Province Doctoral Research Start-up Fund Project (2020-BS-282); and the Key Planned Project of Year 2020 of Department of Science & Technology of Liaoning Province

**Table 2**
The response related DEPs of *Escherichia coli* O157:H7 after AMAs treatment.

| Protein ID | Gene | Description | Change | Protein ID | Gene | Description | Change |
|---|---|---|---|---|---|---|---|
| *Mechanical stress and heat shock response* | | | | | | | |
| B1X6E2 | mscL | Large-conductance mechanosensitive channel | Up | B1XDP7 | groL | 60 kDa chaperonin | Down |
| P0C0S1 | mscS | Small-conductance mechanosensitive channel | Down | B7NE05 | hslO | 33 kDa chaperonin | Down |
| P0AEB5 | ynaI | Low conductance mechanosensitive channel YnaI | Down | P0ACH0 | hslR | Heat shock protein 15 | Down |
| B7NQY6 | ibpB | Small heat shock protein IbpB | Up | A7ZIN3 | htpG | Chaperone protein HtpG | Down |
| C5A1D4 | groS | 10 kDa chaperonin | Down | B7MVV9 | htpX | Protease HtpX | Down |
| *Carbohydrate metabolic and energy metabolism* | | | | | | | |
| P00490 | malP | Maltodextrin phosphorylase | Up | P0AFG4 | sucA | 2-oxoglutarate dehydrogenase E1 component | Up |
| P0AC86 | glgP | Glycogen phosphorylase | Up | P00363 | frdA | Fumarate reductase flavoprotein subunit | Up |
| P77475 | yqaB | Fructose-1-phosphate phosphatase YqaB | Up | P0ACX5 | fumD | Fumarase D | Up |
| P31467 | yieH | 6-phosphogluconate phosphatase | Up | P42632 | tdcE | PFL-like enzyme TdcE | Up |
| P36683 | acnB | Aconitate hydratase B | Up | A8A036 | maeA | NAD-dependent malic enzyme | Up |
| P08997 | aceB | Malate synthase A | Down | | | | |
| *Amino acid biosynthesis and metabolism* | | | | | | | |
| A1AID8 | argH | Argininosuccinate lyase | Up | B1XAH6 | dapF | Diaminopimelate epimerase | Down |
| P00370 | gdhA | NADP-specific glutamate dehydrogenase | Up | Q9S5G5 | hisB | Histidine biosynthesis bifunctional protein HisB | Down |
| P13009 | metH | Methionine synthase | Up | P06988 | hisD | Histidinol dehydrogenase | Up |
| B1LRA3 | msrA | Peptide methionine sulfoxide reductase MsrA | Up | P0AD97 | livJ | Leu/Ile/Val-binding protein | Up |
| *Lipid metabolism and transport* | | | | | | | |
| P0AEK5 | fabI | Enoyl-[acyl-carrier-protein] reductase [NADH] FabI | Down | P76506 | mlaA | Intermembrane phospholipid transport system lipoprotein MlaA | Up |
| P0A953 | fabB | 3-oxoacyl-[acyl-carrier-protein] synthase 1 | Down | P60753 | msbA | Lipid A export ATP-binding/permease protein MsbA | Up |
| P0AGG3 | tesB | Acyl-CoA thioesterase 2 | Down | | | | |

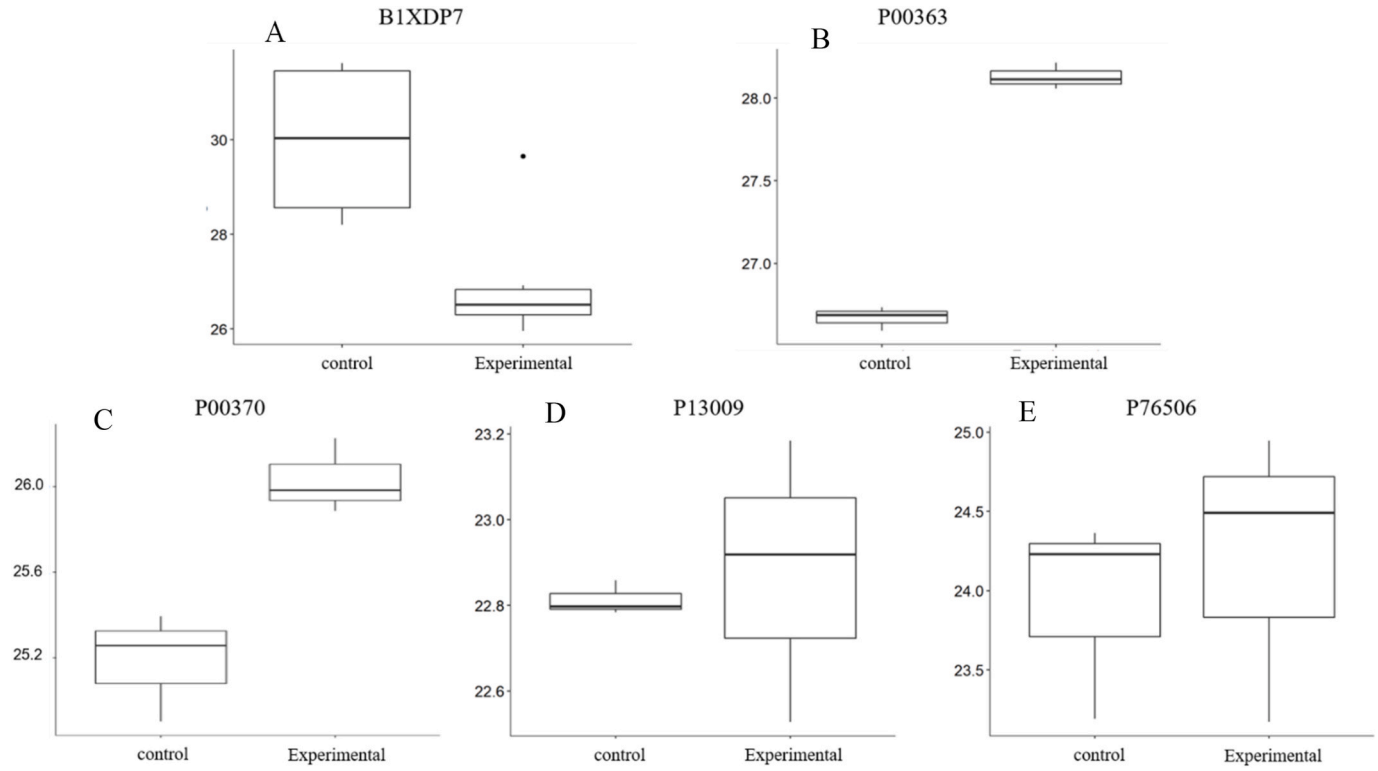


**Fig. 9.** The results of TMT proteomics were verified by MRM. The protein was quantified by peptide segments to draw a box-plot. The box in the experimental group was higher than that in the control group, indicating that the protein was up-regulated; the box in the experimental group was lower than that in the control group, indicating that the protein was down-regulated.

**Table 3**
Comparison of TMT and MRM quantification results.

| UniProt accession | Description | Exp/Con (TMT) | Exp/Con (MRM) |
|---|---|---|---|
| B1XDP7 | 60 kDa chaperonin | 0.41 | 0.41 |
| P00363 | Fumarate reductase flavoprotein subunit | 2.09 | 17.46 |
| P00370 | NADP-specific glutamate dehydrogenase | 3.57 | 2.55 |
| P13009 | Methionine synthase | 3.94 | 1.54 |
| P76506 | Intermembrane phospholipid transport system lipoprotein | 1.90 | 8.25 |

(2020JH2/10200039).

## CRediT authorship contribution statement

**Haotian Deng:** Data curation, Writing – original draft, Preparation. **Yanwen Kong:** Conceptualization. **Jinyan Zhu:** Software, Investigation. **Xinyao Jiao:** Data curation. **Yuqi Tong:** Writing – review & editing. **Meizhi Wan:** Supervision. **Yang Zhao:** Software. **Sixu Lin:** Validation. **Yan Ma:** Software. **Xianjun Meng:** Supervision, Writing – review & editing.

## Declaration of competing interest

The authors declare that they have no known competing financial interests or personal relationships that could have appeared to influence the work reported in this paper.

## Appendix A. Supplementary data

Supplementary data to this article can be found online at https://doi.org/10.1016/j.crfs.2022.09.017.

## References

Alexandrino, T.D., da Silva, M.G., Ferrari, R.A., Ruiz, A.L.T.G., Duarte, R.M.T., Simabuco, F.M., Bezerra, R.M.N., Pacheco, M.T.B., 2021. Evaluation of some in vitro bioactivities of sunflower phenolic compounds. Curr. Res. Food Sci. 4, 662–669. https://doi.org/10.1016/j.crfs.2021.09.007.

Bi, X., Wang, Y., Hu, X., Liao, X., 2017. iTRAQ-based proteomic analysis of sublethally injured Escherichia coli O157:H7 cells induced by high pressure carbon dioxide. Front. Microbiol. 8 https://doi.org/10.3389/fmicb.2017.02544.

Bradford, M.M., 1976. A rapid and sensitive method for the quantitation of microgram quantities of protein utilizing the principle of protein-dye binding. Anal. Biochem. 72, 248–254. https://doi.org/10.1016/0003-2697(76)90527-3.

Denev, P., Ciz, M., Kratchanova, M., Blazheva, D., 2019. Black chokeberry (Aronia melanocarpa) polyphenols reveal different antioxidant, antimicrobial and neutrophil-modulating activities. JUN.30 Food Chem. 284, 108–117. https://doi.org/10.1016/j.foodchem.2019.01.108.

Deng, H., Zhu, J., Tong, Y., Kong, Y., Tan, C., Wang, M., Wan, M., Meng, X., 2021. Antibacterial characteristics and mechanisms of action of Aronia melanocarpa anthocyanins against Escherichia coli. LWT–Food Sci. Technol. 150 https://doi.org/10.1016/j.lwt.2021.112018.

Efenberger-Szmechtyk, M., Nowak, A., Czyowska, A., Niadowska, M., Yelewicz, D., 2021. Antibacterial mechanisms of Aronia melanocarpa (Michx.), Chaenomeles superba Lindl. and Cornus mas L. leaf extracts. Food Chem., 129218 https://doi.org/10.1016/j.foodchem.2021.129218.

Gao, M.-M., Hu, F., Zeng, X.-D., Tang, H.-L., Zhang, H., Jiang, W., Yan, H.-J., Shi, H., Shu, Y., Long, Y.-S., 2020. Hypothalamic proteome changes in response to nicotine and its withdrawal are potentially associated with alteration in body weight. J. Proteonomics 214. https://doi.org/10.1016/j.jprot.2020.103633.

Gao, X., Yin, Y., Wu, H., Hao, Z., Liu, Y., 2020. Integrated SERS platform for reliable detection and photothermal elimination of bacteria in whole blood samples. Anal. Chem. 93 (3) https://doi.org/10.1021/acs.analchem.0c03981.

Gong, S., Richard, H., Foster, J.W., 2003. YjdE (AdiC) is the arginine:agmatine antiporter essential for arginine-dependent acid resistance in Escherichia coli. J. Bacteriol. 185 (15), 4402–4409. https://doi.org/10.1128/JB.185.15.4402-4409.2003.

Hesslinger, C., Fairhurst, S.A., Sawers, G., 1998. Novel keto acid formate-lyase and propionate kinase enzymes are components of an anaerobic pathway in Escherichia coli that degrades L-threonine to propionate. Mol. Microbiol. 27 (2), 477–492. https://doi.org/10.1046/j.1365-2958.1998.00696.x.

Higbee, J., Solverson, P., Zhu, M., Carbonero, F., 2022. The emerging role of dark berry polyphenols in human health and nutrition. Food Front. 3, 3–27. https://doi.org/10.1002/fft2.128.

John, D., Ramaswamy, H.S., 2020. Comparison of pulsed light inactivation kinetics and modeling of Escherichia coli (ATCC-29055), Clostridium sporogenes (ATCC-7955) and Geobacillus stearothermophilus (ATCC-10149). Curr. Res. Food Sci. 3, 82–91. https://doi.org/10.1016/j.crfs.2020.03.005.

Kang, S., Shi, C., Chang, J., Kong, F., Li, M., Guan, B., Zhang, Z., Shi, X., Zhao, H., Peng, Y., Zheng, Y., Yue, X., 2021. Label free-based proteomic analysis of the food spoiler Pseudomonas fluorescens response to lactobionic acid by SWATH-MS. Food Control 123. https://doi.org/10.1016/j.foodcont.2020.107834.

Kong, Y., Yan, T., Tong, Y., Deng, H., Wang, Y., 2021. Gut microbiota modulation by polyphenols from Aronia melanocarpa of LPS-induced liver diseases in rats. J. Agric. Food Chem. 69 (11), 3312–3325. https://doi.org/10.1021/acs.jafc.0c06815.

Kuczynska-Wisnik, D., Zurawa-Janicka, D., Narkiewicz, J., Kwiatkowska, J., Lipinska, B., Laskowska, E., 2004. Escherichia coli small heat shock proteins IbpA/B enhance activity of enzymes sequestered in inclusion bodies. Acta Biochim. Pol. 51 (4), 925–931.

Kuznetsova, E., Proudfoot, M., Gonzalez, C.F., Brown, G., Omelchenko, M.V., Borozan, I., Carmel, L., Wolf, Y.I., Mori, H., Savchenko, A.V., Arrowsmith, C.H., Koonin, E.V., Edwards, A.M., Yakunin, A.F., 2006. Genome-wide analysis of substrate specificities of the Escherichia coli haloacid dehalogenase-like phosphatase family. J. Biol. Chem. 281 (47), 36149–36161. https://doi.org/10.1074/jbc.M605449200.

Kwon, Y.I., Apostolidis, E., Labbe, R.G., Shetty, K., 2007. Inhibition of Staphylococcus aureus by phenolic phytochemicals of selected clonal herbs species of lamiaceae family and likely mode of action through proline oxidation. Food Biotechnol. 21 (1), 71–89. https://doi.org/10.1080/08905430701191205.

Lacombe, A., Wu, V., Tyler, S., Edwards, K., 2010. Antimicrobial action of the American cranberry constituents; phenolics, anthocyanins, and organic acids, against Escherichia coli O157:H7. Int. J. Food Microbiol. 139 (1–2), 102–107. https://doi.org/10.1016/j.ijfoodmicro.2010.01.035.

Lacombe, A., Mcgivney, C., Tadepalli, S., Sun, X., Wu, V., 2013. The effect of American cranberry (Vaccinium macrocarpon) constituents on the growth inhibition, membrane integrity, and injury of Escherichia coli O157:H7 and Listeria monocytogenes in comparison to Lactobacillus rhamnosus. Food Microbiol. 34 (2), 352–359. https://doi.org/10.1016/j.fm.2013.01.008.

Li, S., Li, L., Zeng, Q., Liu, J., Yang, Y., Ren, D., 2018. Quantitative differences in whey proteins among Murrah, Nili-Ravi and Mediterranean buffaloes using a TMT proteomic approach. Food Chem. 269, 228–235. https://doi.org/10.1016/j.foodchem.2018.06.122.

Li, J., Zhang, X., Ashokkumar, M., Liu, D., Ding, T., 2020. Molecular regulatory mechanisms of Escherichia coli O157:H7 in response to ultrasonic stress revealed by proteomic analysis. Ultrason. Sonochem. 61 https://doi.org/10.1016/j.ultsonch.2019.104835.

Lim, J.S., Ha, J.W., 2021. Growth temperature influences the resistance of Escherichia coli O157:H7 and Salmonella enterica serovar Typhimurium on lettuce to X-ray irradiation. Food Microbiol. 99 (7), 103825 https://doi.org/10.1016/j.fm.2021.103825.

Lingshuai, Meng, Guang, Xin, Bin, Li, Dongnan, Xiyun, Sun, Tingcai, 2018. Anthocyanins extracted from Aronia melanocarpa protect SH-SY5Y cells against amyloid-beta (1-42)-induced apoptosis by regulating Ca2+ homeostasis and inhibiting mitochondrial dysfunction. J. Agric. Food Chem. 66 (49), 12967–12977. https://doi.org/10.1021/acs.jafc.8b05404.

Liu, X., Tang, J., Wang, L., Giesy, J.P., 2018. Mechanisms of oxidative stress caused by CuO nanoparticles to membranes of the bacterium Streptomyces coelicolor M145. Ecotoxicol. Environ. Saf. 158, 123–130. https://doi.org/10.1016/j.ecoenv.2018.04.007.

Malinverni, J.C., Silhavy, T.J., 2009. An ABC transport system that maintains lipid asymmetry in the Gram-negative outer membrane. Proc. Natl. Acad. Sci. U. S. A 106 (19), 8009–8014. https://doi.org/10.1073/pnas.0903229106.

Mogk, A., Mayer, M.P., Deuerling, E., 2002. Mechanisms of protein folding: molecular chaperones and their application in biotechnology. Chembiochem : Eur. J. Chem. Biol. 3 (9), 807–814. https://doi.org/10.1002/chin.200246272.

Molina, I., Pellicer, M., iacute, a-Teresa, Badia, J., Aguilar, J., Baldoma, L., 2010. Molecular characterization of Escherichia coli malate synthase G. Differentiation with the malate synthase A isoenzyme. FEBS J. 224 (2), 541–548. https://doi.org/10.1111/j.1432-1033.1994.00541.x.

Moreira Gonçalves, S., Gomes Motta, J.F., Ribeiro-Santos, R., Hidalgo Chávez, D.W., Ramos de Melo, N., 2020. Functional and antimicrobial properties of cellulose acetate films incorporated with sweet fennel essential oil and plasticizers. Curr. Res. Food Sci. 3, 1–8. https://doi.org/10.1016/j.crfs.2020.01.001.

Ning, Y., Fu, Y., Hou, L., Ma, M., Wang, Z., Li, X., Jia, Y., 2021. iTRAQ-based quantitative proteomic analysis of synergistic antibacterial mechanism of phenyllactic acid and lactic acid against Bacillus cereus. Food Res. Int. 139 https://doi.org/10.1016/j.foodres.2020.109562.

Ohtomo, T., Nakao, C., Sumiya, M., Kaminuma, O., Abe, A., Mori, A., Inaba, N., Kato, T., Yamada, J., 2013. Identification of acyl-CoA thioesterase in mouse mesenteric lymph nodes. Biol. Pharmaceut. Bull. 36 (5), 866–871. https://doi.org/10.1248/bpb.b12-01088.

Paes, J.A., Leal Zimmer, F.M.A., Moura, H., Barr, J.R., Ferreira, H.B., 2019. Differential responses to stress of two Mycoplasma hyopneumoniae strains. J. Proteonomics 199, 67–76. https://doi.org/10.1016/j.jprot.2019.03.006.

Righi, N., Boumerfeg, S., Fernandes, P., Deghima, A., Baghiani, A., 2020. Thymus algeriensis Bioss & Reut: relationship of phenolic compounds composition with in vitro/in vivo antioxidant and antibacterial activity. Food Res. Int. 136, 109500 https://doi.org/10.1016/j.foodres.2020.109500.

Sarengaowa, Hu, W., Feng, K., Xiu, Z., Jiang, A., Lao, Y., 2019. Tandem mass tag-based quantitative proteomic analysis reveal the inhibition mechanism of thyme essential oil against flagellum of Listeria monocytogenes. Food Res. Int. 125 https://doi.org/10.1016/j.foodres.2019.108508.

Sengun, I.Y., Kilic, G., Ozturk, B., 2020. The effects of koruk products used as marination liquids against foodborne pathogens (Escherichia coli O157:H7, Listeria monocytogenes and Salmonella Typhimurium) inoculated on poultry meat. LWT (Lebensm.-Wiss. & Technol.) 133. https://doi.org/10.1016/j.lwt.2020.110148.

Elwira, Sieniawska, Maciejewska-Turska, Magdalena, Świątek, Łukasz, Xiao, Jianbo, 2020. Plant-based food products for antimycobacterial therapy. eFood 1 (3), 199–216. https://doi.org/10.2991/efood.k.200418.001.

Sr, A., So, B., Mrp, A., Wjl, A., By, A., Hjc, A., Mho, C., Nso, D., Mhs, E., Yk, F., 2019. Pathogenesis of Enterohemorrhagic Escherichia coli O157:H7 is mediated by the cytochrome P450 family in Caenorhabditis elegans animal model. Food Control 103, 182–185. https://doi.org/10.1016/j.foodcont.2019.03.036.

Sun, X.H., Zhou, T.T., Wei, C.H., Lan, W.Q., Zhao, Y., Pan, Y.J., Wu, V., 2018. Antibacterial effect and mechanism of anthocyanin rich Chinese wild blueberry extract on various foodborne pathogens. Food Control 94, 155–161. https://doi.org/10.1016/j.foodcont.2018.07.012.

Tan, C., Li, D., Wang, H., Tong, Y., Zhao, Y., Deng, H., Kong, Y., Shu, C., Yan, T., Meng, X., 2021. Effects of high hydrostatic pressure on the binding capacity, interaction, and antioxidant activity of the binding products of cyanidin-3-glucoside and blueberry pectin. Food Chem. 344 https://doi.org/10.1016/j.foodchem.2020.128731.

Tasic, N., Jakovljevic, V., Mitrovic, M., Djindjic, B., Turnic, T.N., 2021. Black chokeberry Aronia melanocarpa extract reduces blood pressure, glycemia and lipid profile in patients with metabolic syndrome: a prospective controlled trial. Mol. Cell. Biochem. 1–11. https://doi.org/10.1007/s11010-021-04106-4.

Usaga, J., Acosta, O., Padilla-Zakour, O.I., Churey, J.J., Worobo, R.W., 2021. Evaluation of high pressure processing (HPP) inactivation of Escherichia coli O157:H7, Salmonella enterica and Listeria monocytogenes in acid and acidified juices and beverages. Int. J. Food Microbiol. 339 (2) https://doi.org/10.1016/j.ijfoodmicro.2020.109034.

Voigt, B., Schroeter, R., Schweder, T., Juergen, B., Albrecht, D., van Dijl, J.M., Maurer, K.-H., Hecker, M., 2014. A proteomic view of cell physiology of the industrial workhorse Bacillus licheniformis. J. Biotechnol. 191, 139–149. https://doi.org/10.1016/j.jbiotec.2014.06.004.

Vougier, S., Mary, J., Friguet, B., 2003. Subcellular localization of methionine sulphoxide reductase A (MsrA): evidence for mitochondrial and cytosolic isoforms in rat liver cells. Biochem. J. 373 (2), 531–537. https://doi.org/10.1042/BJ20030443.

Wang, H., Xie, Y., Zhang, H., Jin, J., Zhang, H., 2020. Quantitative proteomic analysis reveals the influence of plantaricin BM-1 on metabolic pathways and peptidoglycan synthesis in Escherichia coli K12. PLoS One 15 (4), e0231975. https://doi.org/10.1371/journal.pone.0231975.

Watson, K.A., Schinzel, R., Palm, D., Johnson, L.N., 1997. The crystal structure of Escherichia coli maltodextrin phosphorylase provides an explanation for the activity without control in this basic archetype of a phosphorylase. EMBO J. 16 (1), 1–14. https://doi.org/10.1093/emboj/16.1.1.

Wesche, A.M., Gurtler, J.B., Marks, B.P., Ryser, E.T., 2009. Stress, sublethal injury, resuscitation, and virulence of bacterial foodborne pathogens. J. Food Protect. 72 (5), 1121–1138. https://doi.org/10.1089/cmb.2008.0161.

Zhu, F.M., Li, J.X., Ma, Z.L., Li, J., Du, B., 2021. Structural identification and in vitro antioxidant activities of anthocyanins in black chokeberry (Aronia melanocarpa lliot). eFood 2 (4), 201–208. https://doi.org/10.53365/efood.k/143829.